

Assessment of thermal comfort in workstations located near highly glazed façades: solar-adjustment models

Avaliação de conforto térmico em estações de trabalho localizadas próximo a fachadas envidraçadas: modelos de ajuste solar

Mônica Martins Pinto 

Fernando Simon Westphal 

Abstract

Although solar radiation exposure strongly impacts people's thermal comfort, workstations are frequently positioned close to glazed façades. Solar adjustment models have been developed to include the solar radiation impact on people's thermal comfort, which the Fanger and Adaptive models do not address. Nonetheless, those models present differences in their calculation procedures, which have not been thoroughly investigated. This study aims to verify differences in thermal comfort results by applying various solar adjustment models of thermal comfort indices for a person sitting close to a highly glazed façade in an office room. The analyses were based on indoor environment data from computer thermal simulations in EnergyPlus for a temperate climate in Brazil. The results for the same room demonstrated significant differences. For example, the hourly difference between the solar-adjustment models reached 1.7 in PMV, and the MRT was up to 17.6 °C higher than the mean result calculated through EnergyPlus. The need for solar radiation incidence control is also reinforced. Although the results were not compared with measurement data or people's thermal perception, the limitations and advantages of each solar adjustment model were numerically analysed, broadening the discussions about the solar adjustment models and the consequences of the choices among them.

Keywords: Solar radiation. Transparent envelope buildings. Thermal comfort model. PMV.

Resumo

Embora a exposição à radiação solar tenha forte impacto no conforto das pessoas, estações de trabalho são frequentemente posicionadas junto às janelas. Modelos de ajuste solar vêm sendo desenvolvidos para incluir o impacto da radiação solar no conforto térmico, o que não é abordado nos modelos de Fanger e Adaptativo. Entretanto, esses modelos apresentam diferenças em seus procedimentos de cálculo, as quais não foram amplamente investigadas. Esse estudo teve como objetivo verificar divergências nos resultados de conforto térmico através da aplicação de diferentes modelos de ajuste solar, considerando uma pessoa sentada próximo à fachada envidraçada em um escritório. Dados ambientais foram obtidos por simulação térmica no EnergyPlus para um clima temperado no Brasil. Observaram-se diferenças significativas nos resultados obtidos para um mesmo espaço. Por exemplo, a diferença horária máxima no PMV entre os modelos de ajuste solar foi 1,7 e a MRT foi até 17,6 °C maior do que o valor médio calculado pelo EnergyPlus. Embora os resultados não tenham sido confrontados com dados de medição ou percepção térmica de pessoas em um ambiente real, as limitações e vantagens de cada modelo de ajuste solar foram analisadas numericamente, ampliando as discussões sobre a necessidade de ajuste solar e as consequências da escolha entre os modelos.

Palavras-chave: Radiação solar. Transparência na envoltória. Modelo de conforto térmico.

¹Mônica Martins Pinto
¹Universidade Federal de Santa Catarina
Florianópolis - SC - Brasil

²Fernando Simon Westphal
²Universidade Federal de Santa Catarina
Florianópolis - SC - Brasil

Recebido em 15/12/21
Aceito em 25/02/22

Introduction

When focusing on heat transfer through the building envelope, concern with glass is emphasized. The window thermal and energy performance depends mainly on its thermal and solar transmittance and system tightness (GASPARELLA *et al.*, 2011). The exchanges are more direct and intense in those elements due to their transparency to solar radiation and high thermal transmittance. For this reason, windows are the building envelope component that most contribute to heat gain and have an impact on the occupants' thermal comfort. However, workstations are often located near windows, where thermal discomfort is more likely to occur.

Although the external view is highly desirable, large glass façades areas could substantially increase the internal thermal load, leading to overheating and increasing cooling demand (HUANG; NIU; CHUNG, 2014). On the other hand, in cold-weather places such as Canada, this heat increase can be beneficial and reduce the heating demand (TZEMPELIKOS *et al.*, 2010). Zygmont and Gawin (2018) emphasize the need to control solar radiation admission to increase indoor thermal comfort and reduce the cooling demand, mainly over the summertime. However, even in lower temperature weather, thermal discomfort by heat is often reported, especially in highly glazed buildings (HAWILA *et al.*, 2018; PINTO; WESTPHAL, 2019; TZEMPELIKOS *et al.*, 2010).

Cappelletti *et al.* (2014) highlighted that the diffuse and direct solar radiation contribution should not be neglected. It is often the cause of occupants' discomfort due to the incidence of beam solar radiation and radiant asymmetry by glass heat absorption. To relieve solar incidence, the occupants tend to activate blinds. Consequently, this fact also increases the energy consumption for artificial light due to the decrease in natural light admission and the increase in artificial system use (BAVARESCO; GHISI, 2017).

Radiant heat exchanges play a relevant role in human thermal balance assessment in indoor and outdoor environments (THORSSON *et al.*, 2007) and represent up to 30% of total heat exchanges in a person (LA GENNUSA *et al.*, 2005). For this reason, solar radiation on the body strongly affects the thermal sensation perceived by the building occupant (MARINO *et al.*, 2017a).

The radiant field is usually represented through the Mean Radiant Temperature (MRT). This index cannot be obtained directly by measurements, and two main methods are used and recommended by standards. The first one calculates the MRT based on the air and globe temperature, accessed from local measurements, which computes the contribution of both long and short-wave radiation without distinguishing them. The second method correlates the temperature of surfaces around the subject with the view factor between person and surfaces. The short-wave radiation component is not included, and it expresses the effect of mean long-wave radiant temperature only. Therefore, this approach evaluates radiant temperature asymmetry due to the window surface temperature but not caused by the direct solar incidence.

Regarding the main international standards concerning thermal comfort in buildings, such as ANSI/ASHRAE 55 (AMERICAN..., 2017), ISO 7730 (INTERNATIONAL..., 2005), ISO 17772-1 (INTERNATIONAL..., 2017), ISO/TR 17772-2 (INTERNATIONAL..., 2018), and EN 16798-1 (BRITISH..., 2019), most compute the infrared portion of the radiation heat exchange. Among them, only ANSI/ASHRAE 55 (AMERICAN..., 2017) considers the contribution of solar radiation on occupants' thermal comfort.

Additionally, the MRT varies depending on the occupant location in the indoor environment, mainly regarding the envelope surfaces' proximity (ZOMORODIAN; TAHSILDOOST, 2017). Moreover, the occupant thermal perception follows this fluctuation, and therefore the thermal comfort assessment in the expected workstation location in office buildings is essential (MARINO *et al.*, 2018a).

Most studies on the effect of window parameter change in the indoor thermal comfort indices applied simplified assessment methods that consider a homogeneous operative temperature or a central room point. Besides that, most studies do not use any adjustment regarding the solar radiation that enters through the windows. Thereby, the chances of local thermal discomfort near the external walls, especially windows, are neglected.

Solar adjustment models of thermal comfort indices

Tools and methods to correct the solar radiation effects in comfort indices have been developed to improve the thermal comfort assessment. Most of these methods correct the MRT and may be applied in both Adaptive and PMV-PPD models (ARENS *et al.*, 2015; LA GENNUSA *et al.*, 2007; MARINO *et al.*, 2018b). They may also be combined with the Two-node model, as in Bessoudo *et al.* (2010) and

Tzempelikoset al. (2010). Zhang et al. (2018) proposed one correction directly in the PMV and one operative temperature adjustment by adding the solar radiation equivalent temperature and a solar radiation coefficient at its ponderation. Huang and Zhai (2020) include solar radiation as an air temperature component and replace it in the PMV equation.

Solar-Adjusted Mean Radiant Temperature (SA-MRT)

The model developed by La Gennusaet al. (2005, 2007) adjusts the MRT considering the radiation incident on the subject by adding beam and diffuse solar radiation components to the heat flow by radiation. This adjustment is indicated for thermally moderate indoor environments, such as office spaces, and it may be applied to both PMV-PPD and Adaptative models. The adjustment considers geometric factors, such as room dimensions, view factors between the subject and surrounding surfaces, solar altitude, and azimuth. In this model, the MRT of the irradiated subject ($T_{r,irr}$) is defined as the quadratic sum of the average radiant temperature of the non-irradiated subject and the increases in the average radiant temperature due to beam and diffuse solar radiation (Equation 1).

$$\bar{T}_{r,irr}^4 = \sum_{N=1}^N F_{p \rightarrow N} T_N^4 + \frac{C_{dn}}{\varepsilon_p \sigma} (\alpha_{irr,d} \sum_{J=1}^M F_{p \rightarrow J} I_{d,J}^{in} + C_S^{in} \alpha_{irr,b} f_p I_{bn}^{in}) \quad \text{Eq. 1}$$

Where:

$F_{p \rightarrow N}$ is the angle factor between the person and the N^{th} isothermal surface;

$F_{p \rightarrow j}$ is angle factor between the person to j^{th} transparent surface;

T_N is the absolute temperature of the N^{th} isothermal surface (K);

C_{dn} is the day–night coefficient (1 = day, 0 = night);

ε_p is emissivity of the human body;

σ is the constante de Stefan-Boltzmann ($5,67 \cdot 10^{-8} \text{ W/m}^2\text{k}^4$);

$\alpha_{irr,d}$ and $\alpha_{irr,b}$ are the relative absorption coefficient to the diffuse and direct solar radiation, respectively;

$I_{d,J}^{in}$ is the intensity of inner diffuse solar radiation through the j^{th} transparent surface (W/m^2);

I_{bn}^{in} : intensity of indoor beam solar radiation (W/m^2);

C_S^{in} is the inner building shading coefficient; and

f_p is the projected area factor.

This model also includes a method for solar adjustment concerning local discomfort assessment due to radiant temperature asymmetry. To do this, the radiant temperature of the irradiated plane is replaced by Equation 2.

$$T_{pr,irr}^4 = \sum_{N=1}^{N+1} F_{p \rightarrow N} T_N^4 + \frac{C_{dn}}{\varepsilon_p \sigma} (\alpha_{irr,dif} \sum_{J=1}^{M+1} F_{p \rightarrow J} I_{d,J}^{in} + C_S^{in} \alpha_{irr,dif} f_p I_{bn}^{in}) \quad \text{Eq. 2}$$

Where $T_{pr,irr}$ is the radiante temperature of irradiated plane (K).

Modified Solar-Adjusted Mean Radiant Temperature (MSA-MRT)

The human body radiative heat exchange model developed by Marino et al. (2017b, 2018c, 2018b; MARINO; NUCARA; PIETRAFESA, 2017) is similar to the method proposed by La Gennusa et al. (2005, 2007) and corrects the MRT. However, this model includes the solar radiation exchanges derived from indoor surface reflections in addition to the short-wave radiation. It is indicated for indoor thermal comfort condition assessment. The adjusted MRT can be described as in Equation 3. As in SA-MRT, MSA-MRT also includes a solar adjustment method in the radiant temperature asymmetry by replacing the temperature in the irradiated plane as in Equation 4.

$$\bar{T}_r^4 = \sum_{N=1}^N F_{p \rightarrow N} T_N^4 + \frac{\alpha_{sw}}{\varepsilon_p \sigma} [\sum_{J=1}^N F_{p \rightarrow J} I_{d,J}^{in} + f_p I_{bn}^{in} + 0,5 \rho_{floor} I_{b,h} + \sum_{N=1}^N \rho_N (\sum_{J=N}^N F_{N-J} I_{d,J}^{in}) F_{p \rightarrow N}] \quad \text{Eq. 3}$$

Where:

\bar{T}_r is the mean radiant temperature (K);

α_{sw} is the short-wave absorbance of the human body;

ρ_{floor} is the reflectance of the pavement;

ρ_N is the reflectance of the N^{th} surface of the envelope;

$I_{b,h}$ is the direct solar radiation that strikes the horizontal surface of the pavement (W/m^2); and

$F_{N \rightarrow j}$ is the angle factor between the N^{th} isothermal surface and the j^{th} transparent surface.

$$T_{pr} = \sqrt[4]{\frac{\alpha_{LW}}{\varepsilon_{AT}} \sum_{N=1}^N F_{AT \rightarrow N} T_N^4 + \frac{\alpha_{SW}}{\varepsilon_{AT\sigma}} \left(\sum_{J=1}^M F_{AT \rightarrow J} I_{d,J}^{in} + I_{b\perp} \right)} \quad \text{Eq. 4}$$

Where:

T_{pr} is the radiante temperature of plane (K);

α_{LW} is the long-wave absorbance of the human body;

ε_{AT} is the emissivity of plane;

$F_{AT \rightarrow N}$ is the angle factor between the plane and the N^{th} isothermal surface;

$F_{AT \rightarrow j}$ is the angle factor between the plane and the j^{th} transparent surface; and

$I_{b\perp}$ is the beam solar radiation in the plane surface (W/m^2).

SolarCal

The model SolarCal (ARENS *et al.*, 2015) is also applied to MRT by adding the solar radiation effect on human body heat gain and comfort. It is a simplified model that intends a quick estimation of solar radiation and is recommended by ASHRAE Standard 55 (AMERICAN..., 2017). The corrected MRT is defined as the sum of long and short-wave MRT – \bar{t}_{rlw} and \bar{t}_{rsw} , respectively (Equation 5). The short-wave calculation is based on the solar heat gain on the human body through the effective radiant field (ERF), as defined in Equation 6.

$$\bar{t}_r = \bar{t}_{rlw} + \bar{t}_{rsw} \quad \text{Eq. 5}$$

$$\text{ERF}_{\text{solar}} = \left[0,5 \cdot f_{\text{eff}} \cdot f_{\text{svv}} (I_{\text{diff}} + I_{\text{TH}} R_{\text{floor}}) + \frac{A_p f_{\text{bes}} I_{\text{bn}}}{A_D} \right] \cdot T_{\text{sol}} \left(\frac{\alpha_{\text{SW}}}{\alpha_{\text{LW}}} \right) \quad \text{Eq. 6}$$

Where:

$\text{ERF}_{\text{solar}}$ is the solar effective radiant field;

f_{eff} is the fraction of the body surface exposed to radiation from the environment;

f_{svv} is the fraction of sky vault exposed to body;

f_{bes} is the fraction of the body exposed to sun;

I_{diff} is the outdoor diffuse sky irradiance on the horizontal plane (W/m^2);

I_{TH} is the total horizontal outdoor solar intensity (W/m^2);

I_{bn} is the direct beam (normal) solar radiation (W/m^2);

R_{floor} is the reflectance of the floor and lower furnishings;

A_p is the projected area (m^2);

A_D is the DuBois surface area of the assumed person, around 1.8 m^2 (m^2); and

T_{sol} is the total solar transmittance, including the glass and shades of a window system (K).

Based on the Kirchhoff law, the absorbed solar heat equals the additional amount of long-wave radiation emitted by the body. Therefore, the ERF is the sum of long-wave and solar ERF and the short-wave MRT is obtained through the ERF on the human body from the long-wave exchange with surfaces.

This model does not include a method for radiant temperature asymmetry. However, Standard 55 (AMERICAN..., 2017), which recommends the SolarCal model for solar-adjustment, also presents an adjustment in the irradiated plane temperature, where \bar{t}_{rsw} is added to the radiant temperature in the plane (t_{pr}) in the irradiated plane.

Corrected Predicted Mean Vote (CPMV)

The Corrected Predicted Mean Vote (CPMV), developed by Zhang *et al.* (2018), includes the influence of solar radiation on thermal comfort through a new component in the PMV calculation. This model is

indicated for indoor environments with solar radiation exposure. The PMV and PPD corrections are defined as Equation 7 and Equation 8, respectively.

$$CPMV = [0.303 \cdot \exp(-0.036 \cdot M) + 0.0275] \cdot \{(M - W) - 3.05 \cdot [5.733 - 0.007 \cdot (M - W) - P_a] - 0.42 \cdot [(M - W) - 58.15] - 1.73 \cdot 10^{-2} \cdot M \cdot (5.867 - P_a) - 0.0014 \cdot M \cdot (34 - t_a) - R_1 + R_b - f_{cl} \cdot h_c \cdot (t_{cl} - t_a)\} \quad \text{Eq. 7}$$

$$PPD = 100 - 95 \cdot e^{[-(0.03353 \cdot CPMV^4 + 0.2179 \cdot CPMV^2)]} \quad \text{Eq. 8}$$

Where:

M is the metabolic rate (W/m²);

W is the effective mechanical power (W/m²);

P_a is the water vapour partial pressure (kPa);

t_a is the indoor air temperature (°C);

f_{cl} is the clothing surface area factor;

h_c is the convective heat transfer coefficient (W/m².K); and

t_{cl} is the clothing surface temperature (°C).

R₁ is the long-wave radiation heat transfer between humans and the surroundings (Equation 9), and R_b is the direct solar radiation heat load per body surface area (Equation 10).

$$R_1 = \left[\varepsilon f_{cl} f_{eff} \sigma \frac{(t_{cl} + 273)^4 - (t_r + 273)^4}{(t_{cl} - t_a)} \right] (t_{cl} - t_a) \quad \text{Eq. 9}$$

$$R_b = \alpha_{sw} f_{cl} f_{eff} f_p I_{bn}^{in} \quad \text{Eq. 10}$$

Afterwards, the authors conducted a field experiment and concluded that the CPMV presents a significant deviation of the thermal sensation votes collected when in high diffuse solar radiation exposition (ZHANG *et al.*, 2020). Therefore, they proposed the CPMV* index, which includes a diffuse solar radiation component (Equation 11). The PPD index was also adjusted following the experiment results. They concluded that only replacing the PMV for CPMV* in the PPD equation would not be consistent due to the variability in solar radiation acceptance. The authors suggest the percentage unacceptable (PPUA), described in Equation 12.

$$R_{diff} = \alpha_{sw} f_{cl} f_{eff} \sum_{j=1}^{N_d} (F_{p \rightarrow j} I_{d,j}^{in}) \quad \text{Eq. 11}$$

$$PPUA = 100 - 88 \exp[-0.00015(CPMV^* + 0.34)^4 - 0.08768(CPMV^* + 0.34)^2] \quad \text{Eq. 12}$$

CPMV and CPMV* models do not indicate any solar adjustment in radiant temperature asymmetry estimation.

Considerations on solar-adjustment models

The solar-adjustment models present significant differences between their calculation methods. The SA-MRT model (LA GENNUSA *et al.*, 2007) was the groundbreaking solar adjustment model that adds the effect of solar radiation incident on the occupant predicted thermal comfort by an MRT correction. The MSA-MRT model (MARINO *et al.*, 2017a) was improved by including the solar radiation flux from short-wave radiation reflected throughout indoor surfaces. The SolarCal (ARENS *et al.*, 2015) uses outdoor solar radiation data easily obtained in weather stations or climate files, facilitating data acquisition. The CPMV model (ZHANG *et al.*, 2018) requires fewer input data, simplifying the procedure, but adheres to PMV adjustment. This model presents a relevant limitation: it includes the beam solar radiation effect only. However, the authors published a model correction, the CPMV*, including a diffuse solar radiation component (ZHANG *et al.*, 2020).

In a recent study, Huang and Zhai (2020) compared the results of thermal comfort obtained by applying nine different solar-adjustment models, including a new proposal with the measurements held in an office room in Lhasa, Tibet (Dwc according to Köppen-Geiger). Among the MRT adjustment models, SA-MRT presented the least convergence with the in loco measurements carried out throughout 72 hours in the winter, characterized by high solar radiation intensity and low air temperature. During peak time, MRT calculated with SA-MRT was about 15 °C lower. Between the models that adjust the PMV directly, the model proposed by the authors showed higher accuracy with the measurement-based PMV, varying up to 0.7. The

CPMV model is not compatible with the loco data, mainly in the peak period when the difference reached 4.0 on the PMV scale. The model MSA-MRT reported a strong correlation with the measurements.

Nonetheless, the study presents a few limitations in the measurement methods that compromise the evaluation of the most accurate or appropriate solar-adjustment model. No air conditioning, heating, or fan device was operated during the measurement period. The presence of an occupant in the room was not clear, even though a person was considered in comfort estimation. Furthermore, five globe thermometers were used, but only one value for MRT, PMV, and operative temperature was analyzed. It is unclear whether an average value or only one point was considered. These devices stood along a centerline perpendicular to the window, and the MRT may significantly vary in the space. It would be essential to verify whether the comfort indices calculation applying these models at different points in space would maintain the described correlations. Besides that, the study was applied to one climate only.

In the presented context, this study aims to verify the divergences in the thermal comfort results by applying various solar adjustments models of thermal comfort indices in an office environment with a high façade transparency ratio in a temperate climate. Results obtained by applying the four models described previously were compared based on data from computer thermal simulation in EnergyPlus software.

Methods

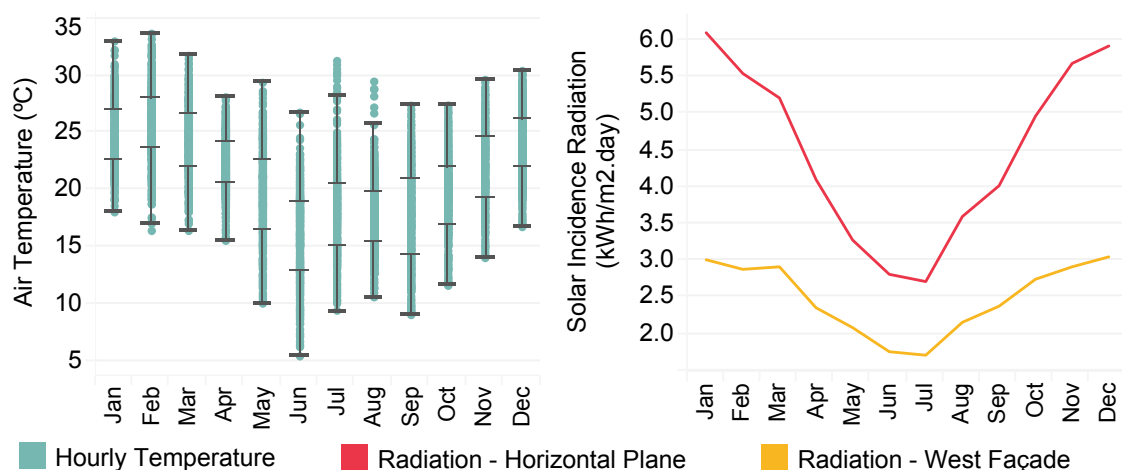
Climate characterization

The study was applied to a coastal town in southern Brazil, Florianópolis. The city presents a Cfa climate, according to Köppen-Geiger, characterized by a temperate climate, well-defined seasons, constantly humid, and hot summers (KOTTEK *et al.*, 2006). Figure 1 shows the monthly statistical data of outdoor air temperature and daily average solar radiation incidence in the horizontal and vertical west planes.

A summer workday with the highest level of solar radiation incident in the West façade was selected: December 6th. The maximum hourly value is 830 W/m², and the daily total is 4.7 kWh/m². Figure 2a shows the hourly outdoor temperature and solar radiation incident in the west façade throughout this day. The direct solar incidence in the west façade occurs from 13h to 19h, and the outdoor temperature presents a range of 7.5 °C.

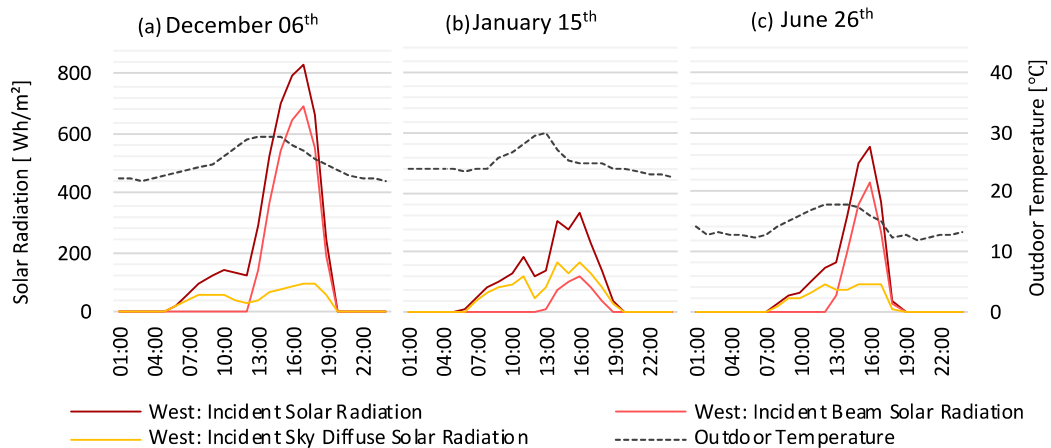
Afterwards, the results of two more days were observed. A summer day, with similar outdoor temperatures on December 6th but low solar radiation incidence, was chosen together with a winter day, with a lower outdoor temperature than December 6th but high solar radiation incidence for the period. The information on the outdoor air temperature and solar radiation incidence in the West façade throughout January 15th and June 26th can be found in Figure 2b and Figure 2c, respectively.

Figure 1 - Florianópolis air temperature and solar radiation incidence



Source: weather file “BRA_Florianopolis.838990_SWERA.epw” (U.S. DEPARTMENT..., 2019).

Figure 2 - Outdoor air temperature and solar radiation incidence in West façade throughout December 6th in Florianópolis



Office model setting

An office room located in an intermediate level was modeled (Figure 3). The room has one external wall, which faces West and presents a WWR (window-to-wall ratio) of 60%. The internal walls, ceiling and floor were set as adiabatic surfaces, assuming that the adjacent rooms and floors have the same thermal conditions. The analyses considered an occupant located 1.5 m from the window. The subject was positioned facing the window considering the critical situation for discomfort.

The internal loads were set according to the recommendations of the Brazilian standard for HVAC design (ABNT, 2008a), assuming a high internal load office profile, with 7.7 m per person, equipment power density 21.5 W/m², and lighting power density 16.0 W/m². The metabolic rate for each occupant was determined according to the ISO 7730 (INTERNATIONAL..., 2005), which is 126 W per person. The same cloth insulation of 0.94 clo was set for all occupants.

Figure 4 shows the occupancy schedule. There is no occupation during weekends, and the artificial lighting system is activated statically without considering the natural light availability.

An HVAC system was modeled as a PTHP (Packaged Terminal Heat Pump) and set according to Table 1. It operates from 7h to 21h and is turned off during weekends. No natural ventilation was modeled since the windows were sealed.

The building has fully glazed facades so that the external walls of each model are covered with the same glass used in the outside window layer. No blind or shadowing device was used. Table 2 presents the opaque constructions and materials' thermal properties.

Six glazing systems were tested to assess the behavior of the solar adjustment models for distinctive glass thermal properties. Three SGU (single glass units) were chosen, covering high, medium, and low solar transmittance. The other three models were configured with IGU (insulated glass unit) constituted by one SGU plus a 12.7 mm air layer and a clear glass. Table 3 shows a summary of their thermal and optical properties.

The glazings' thermal transmittance and SHGC (Solar Heat Gain Coefficient) and the IGU composition properties were calculated using the WINDOW 7.7 software (LAWRENCE..., 2020). However, these values are presented as a reference only. For the energy simulation, each glass layer was modeled in the EnergyPlus with its spectral average optical properties. The glass materials were individually inserted into the EnergyPlus model, and the software adjusted the optical properties according to the solar inclination. To understand the results, the name of each glass composition is a combination of the window system (SGU or IGU) and the rounded SHGC value of the base glass.

Thermal simulation and thermal comfort assessment

The solar-adjustment models previously described were compared considering the thermal behavior of the room by using different glazings. The adjustments were calculated by both CPMV and CPMV* to verify the impact of diffuse solar radiation.

The models need input data related to the outdoor and indoor thermal conditions. Therefore, environment data were obtained through thermal simulations in EnergyPlus v.8.9. Calculations of adjusted MRT, PMV, and PPD indices and radiant temperature asymmetry used the output data from the thermal simulations. The models were inserted in electronic spreadsheets for the determination of the adjusted indices, except for PMV and PPD. The latter were calculated using the CBE Thermal Comfort Tool (TARTARINI *et al.*, 2020). The estimated values were reinserted into the electronic spreadsheets.

Figure 3 - Office floor plan and section plane

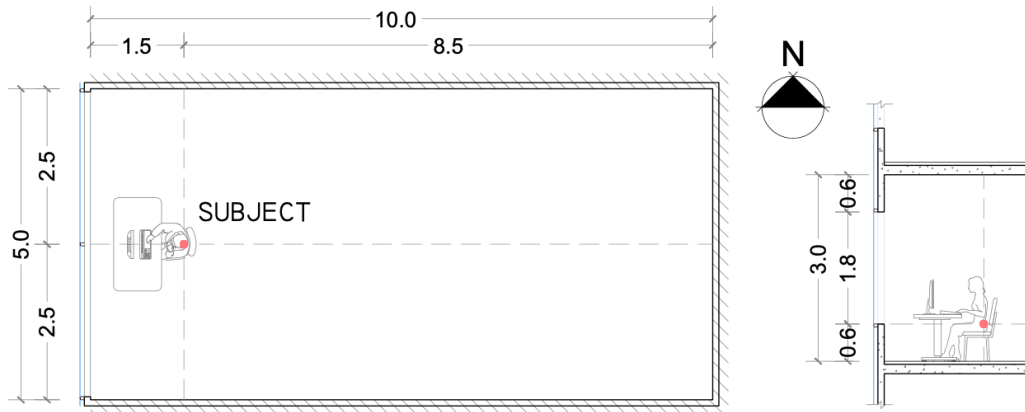


Figure 4 - Workday schedule occupancy

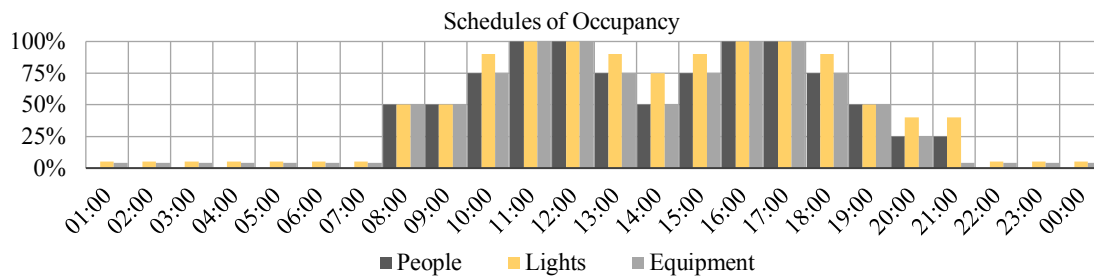


Table 1 - HVAC system characteristics

System	PTHP
Gross Rated COP	3.0 W/W
Capacity	Auto sized by EnergyPlus
Outdoor air	0.0075 m ³ /s per person
Setpoints	Heating: 20°C and Cooling: 24°C
Infiltration rate	0.3 air changes per hour

Table 2 - Thermal properties of constructions

Composition	U-Value (W/m ² .K)	Solar Absorptance	Heat Capacity (kJ/m ² .K)
Exterior Walls			
Plasterboard (12.5mm) + Glass wool (50mm) + Cement board (10mm)	0.77	Indoor: 0.297 Outdoor: 0.297	24.31
Interior Walls (around the core zone only)			
Plasterboard (15mm) + Glass wool (50mm) + Plasterboard (15mm)	0.69	0.297	25.55
Ceiling / Floor			
Mortar (25mm) + Concrete slab (200mm) + Mortar (25mm) + Ceramic floor (7.5mm)	2.74	Ceiling: α=0.297 Floor: α=0.418	551.04

Table 3 - Optical and thermal properties of glass

	SGU30	SGU50	SGU80	IGU30	IGU50	IGU80
Thickness [mm]	8.00	8.00	6.00	26.7	26.7	24.7
T_{sol}	0.11	0.41	0.78	0.09	0.32	0.60
α_{sol}	0.73	0.42	0.15	0.75	0.50	0.29
Manufacturing Process	Laminated	Laminated	Monolithic	Insulated: double- glass	Insulated: double- glass	Insulated: double- glass
U-value [W/m K]	5.56	5.56	5.60	2.71	2.71	2.68
SHGC	0.28	0.51	0.82	0.22	0.43	0.71

In addition to the results calculated with the solar-adjustment models, the thermal comfort indices calculated by the EnergyPlus engine were also presented because this method is recurrent when predicting thermal comfort assessment through computer simulation. The Fanger model was set as the thermal comfort model with the MRT calculation default of EnergyPlus, in which an average point in the room and the MRT is “[...] calculated based on an area-emissivity weighted average of all the surfaces in the zone [...]” (DEPARTMENT..., 2020, p. 488), as expressed in Equation 13.

$$\bar{t}_r = \frac{\sum \epsilon_N A_N t_N}{\sum \epsilon_N A_N} \quad \text{Eq. 13}$$

Where ϵ_N is the emissivity of a internal surface and A_N is its surface area.

Results

Mean Radiant Temperature (MRT)

Figure 5 presents the MRT variation throughout one day by applying the solar-adjustment models per type of glass tested. The dark dashed vertical lines delimit the office occupancy period, and the gray area indicates the period when the solar beam radiation reaches the window façade. CPMV and CPMV* results are not shown here as their corrections are made directly in the PMV index.

As expected, the building model with clear glass was more sensitive to the solar-adjustment models due to its high solar transmittance, i.e., it allows a higher solar radiation fraction to enter through the window. The solar transmittance of clear glass (SGU80) is more than eight times greater than the IGU30.

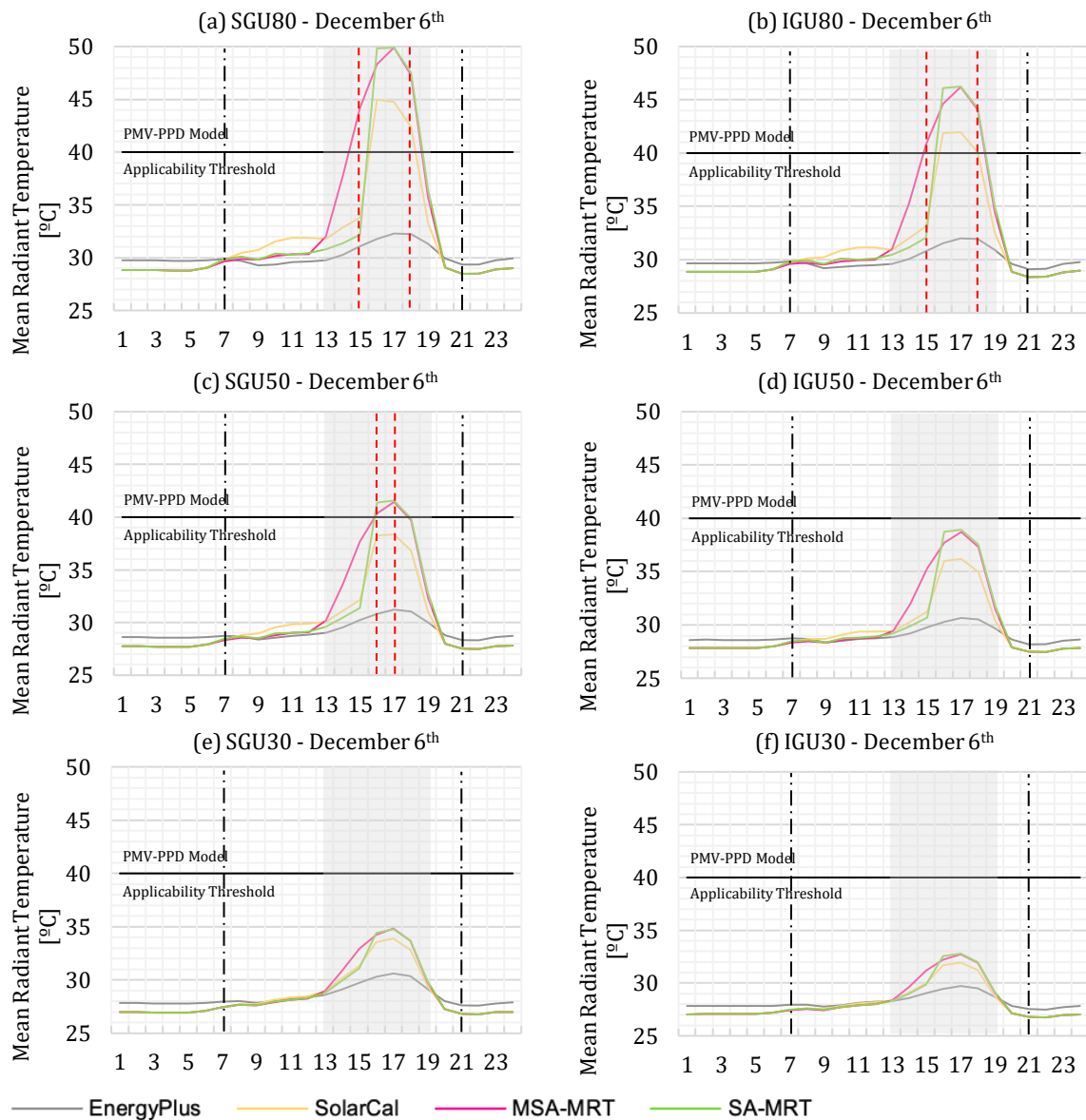
The MSA-MRT and SA-MRT models presented higher sensitivity to the intensity variation of beam solar radiation. The MRT with these models was 17.6 °C higher than calculated by EnergyPlus in the peak of the solar radiation exposure (SGU80 at 17h). The SolarCal model also presented meaningful sensitivity, up to 13.2 °C higher than the EnergyPlus. Among the offices with IGU, the contrast with EnergyPlus was also massive but lower. The highest difference was 14.6 °C with IGU80 when applying MSA-MRT in these cases.

Between 16h and 18h, the MRT remains above the applicability threshold of the PMV-PPD thermal comfort model for all solar-adjustment models (SGU80 and IGU80). However, the MRT exceeds this threshold an hour earlier with the MSA-MRT model. The threshold is also reached in the office model SGU50, between 16h and 17h, by applying SA-MRT and MSA-MRT. The red dashed lines indicate these periods in the graphs (a), (b), and (c) in Figure 5.

SolarCal presented the highest sensitivity to diffuse solar radiation and tends to report increased MRT in the period without direct solar radiation incidence in the West façade (from 6h to 12h). The hourly difference reaches 1.6 °C compared with MSA-MRT and 2 °C with EnergyPlus (SGU80). SA-MRT and MSA-MRT models presented similar MRT when only in diffuse solar radiation presence, in which 0.4 °C is the maximal hourly difference (SGU50). However, this pattern occurred mainly in building models that admitted a higher solar radiation percentage. The solar-adjustment models tend to present similar results to EnergyPlus when using lower SHGC glass.

When the beam solar radiation reaches the subject, SolarCal and SA-MTR tend to maintain the same curve shape, but SolarCal presents a temperature peak between 1 °C and 5 °C lower (IGU30 and SGU80). The similarity results from the two models using external solar radiation data in their calculations.

Figure 5 - Mean Radiant Temperature on December 6th in Florianópolis



On the other hand, MSA-MRT directly considers the radiation that reaches the subject and does not present calculation procedures for the direct solar radiation in the horizontal plane, for the direct solar radiation that reaches the subject and for the diffuse sky radiation that enters the environment through the window. For that reason, EnergyPlus data of solar radiation transmitted through the window was considered in the MSA-MRT calculations.

Further analysis also sought to understand whether the reduction in MRT in insulated glass results from the reduction in U-value or if it is a consequence of the reduction in the transmittance of solar energy. To do this, the internal temperature of the glass was verified (Figure 6).

A tendency opposite to the MRT is noted in the glass surface temperatures. The increase in the window insulation does not necessarily lead to lower temperatures in the interior glass surface. In the SHGC 80 office model, the peak temperature of the glass inner face was 6 °C higher with the IGU system. Conversely, in the models with lower SHGC, the temperature peak was 8 °C lower with IGU.

Furthermore, the results show a tendency that the higher the SHGC, the higher the MRT, but the lower the peak temperature of the inner glass surface. In the office model with SGU80 glass, the MRT reached 49.9 °C by applying SA-MRT and MSA-MRT, and 32.3 °C when calculated by EnergyPlus, while the glass temperature is 34.3 °C (17h). At the same hour in the SGU30 office, the MRT was 34.8 °C when estimated

by SA-MRT and MSA-MRT, and 30.6 °C by EnergyPlus, while the inside face glass temperature was 52.4 °C. The models with IGU tend to present an opposite tendency.

Figure 5 shows a clear reduction in the MRT comparing SGU and IGU. However, this pattern did not recur in the inner glass surface temperature. The internal glass temperature tends to be higher in the IGU models. Considering the base glass with the highest SHGC (SGU80 and IGU80), the inner glass surface temperature is up to 6 °C higher in the IGU system. On the other hand, when the models with the lowest SHGC base glass (SGU30 and IGU30) are analyzed, the IGU model tends to present a lower inner surface temperature (up to 8 °C). The indoor surface temperature tends to be close in both glass systems (SGU and IGU) with a median SHGC glass. The contrast of the inner glass surface temperature is explained by the glazings' solar absorptance and U-value (Table 3). Among this sample, the higher the SHGC, the less the α_{sol} , while the glasses with lower SHGC have a high α_{sol} . The latter consequently tend to absorb more solar radiation and hold the heat gained by conduction, which results in higher temperatures on the inner glass surface. Since the internal walls, floor, and ceiling were set as adiabatic surfaces, the room does not lose heat through these surfaces, and its temperatures tend to remain slightly higher than the indoor air temperature during the whole period.

These results show a tendency that, when choosing an SHGC 80 glass, the best option would be the SGU, which allows better internal load heat dissipation. However, the occupant may experience local discomfort from direct solar radiation incidence when close to the window. The increase in the window thermal transmittance is ineffective in improving the thermal comfort conditions in the environment without reducing solar transmission, especially in climates with high solar incidence.

All solar-adjustment models presented the same values for MRT in periods without diffuse or beam solar radiation incidence because all of them use the same long-wave MRT calculation (INTERNATIONAL..., 1998). However, they reported MRT lower than EnergyPlus results. Figure 7 shows the difference between the long-wave MRT calculated in the room's central point and the person point (1.5m from the window), and both of them are compared with EnergyPlus results.

Figure 6 - Temperature of indoor surfaces on December 6th in Florianópolis

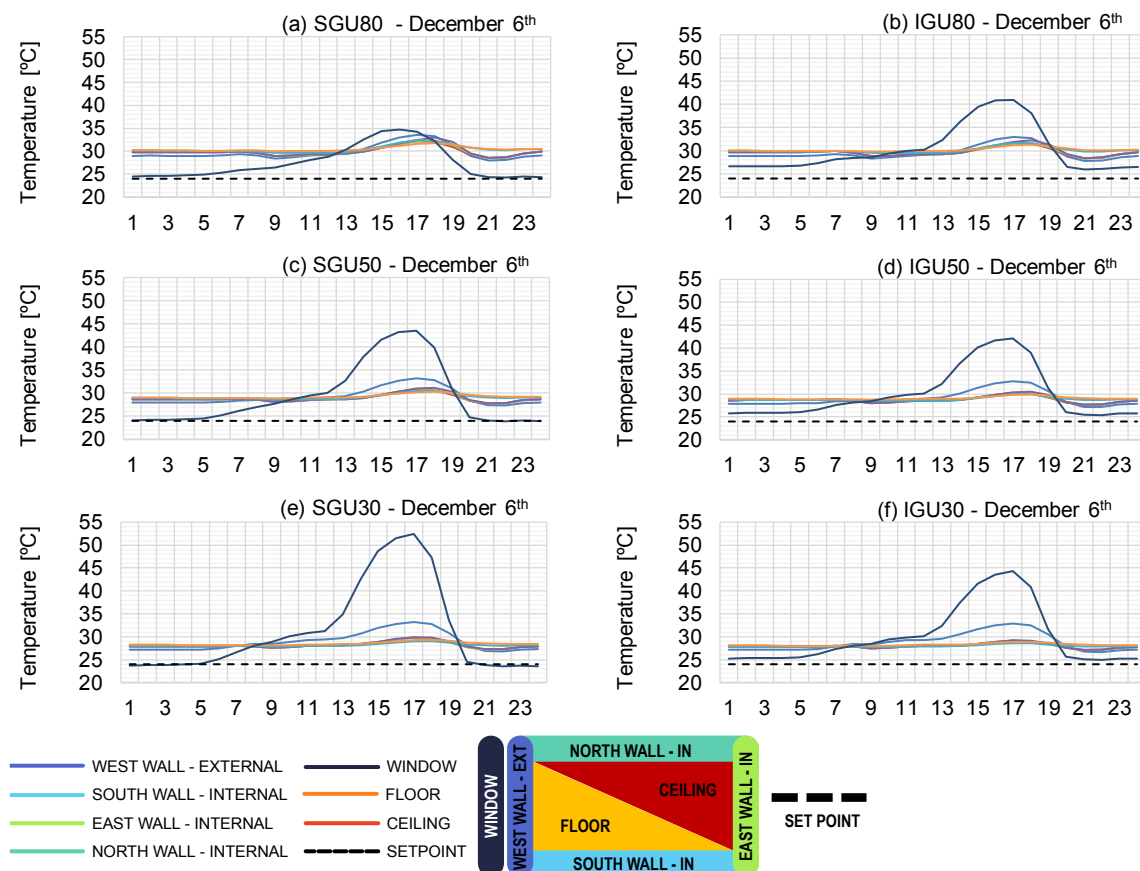
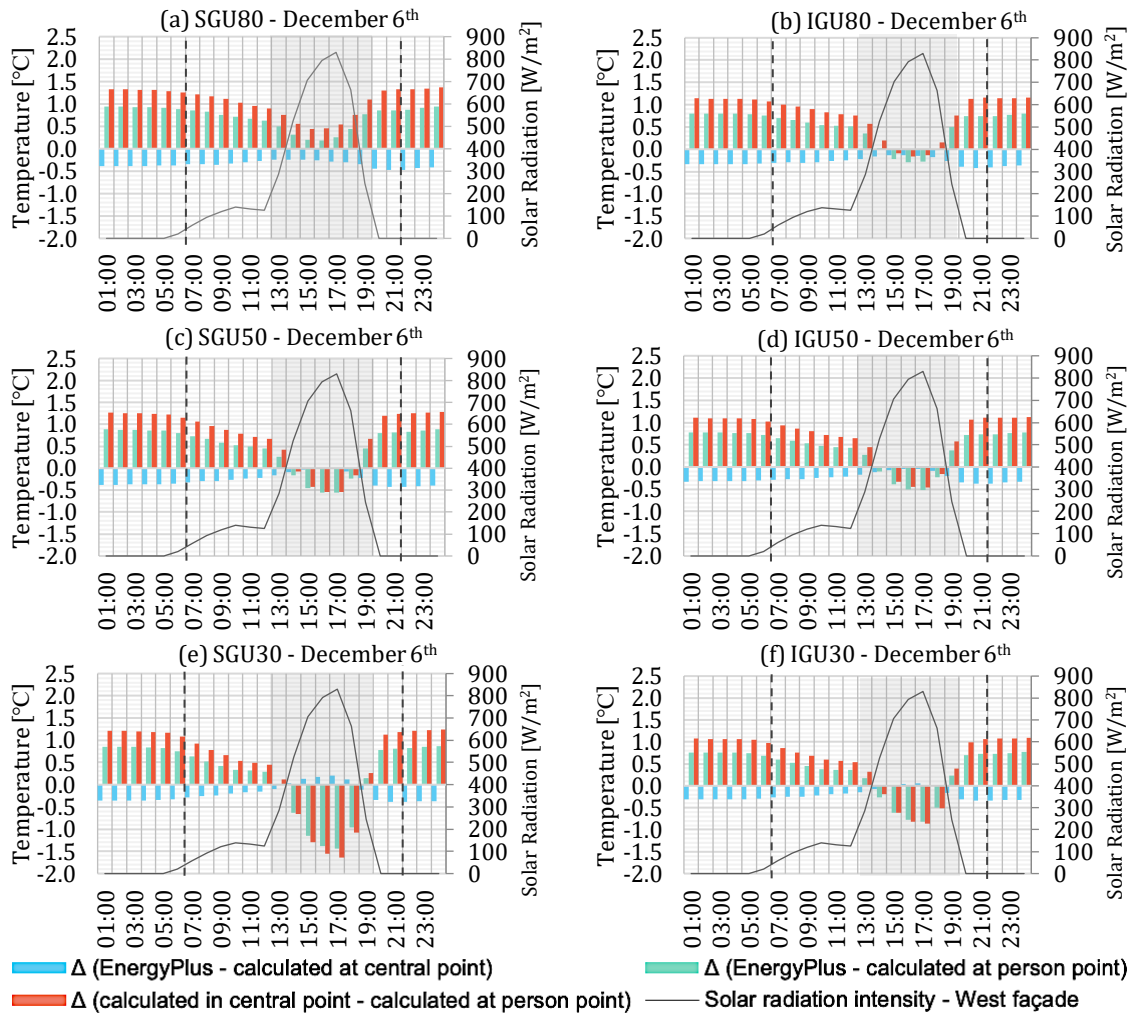


Figure 7 - Difference of long-wave MRT estimation between (1) EnergyPlus and calculated at the room's central point; (2) EnergyPlus and calculated at the person point; and (3) calculated at the room's central point and at the person point



First, the MRT calculated in the room center point is not the same as the EnergyPlus report. It happened because, instead of applying the long-wave MRT calculation considering the indoor surface temperatures and the view factors between the subject and surfaces, EnergyPlus simplifies the MRT calculation as an area-emissivity weighted average of the room surfaces (Equation 13).

Besides that, in the period without beam solar radiation incidence on the window, most office models presented lower MRT near the window than in the center of the room. This occurs due to the lower glass temperature and the heat losses through the window. However, as expected, this tends to change when beam solar radiation reaches the West façade, except for the clear glasses (SGU80 and IGU80). In the SGU80 model, the MRT close to the window remains lower than in the center of the room. In IGU80, the MRT in a point 1.5 m from the window is slightly higher than in a center point (up to 0.3 °C) only between 14h and 17h.

The MRT is calculated based on surface temperature and view factor, representing each surface's influence in the long-wave radiant exchange with the body. Table 4 shows a comparison between the SGU80 and SGU30 models at 17h. The window's inside face temperature in SGU80 is 1.9 °C higher than the average temperature of other surfaces, while this difference is 22.3 °C in the SGU30 model. Besides, even at point 1.5 m from the window, the window temperature influence is significantly lower than the indoor opaque surfaces. When this temperature is too close to others, and the view factor is considerably lower than the sum of the temperatures of the opaque indoor surfaces, the long-wave MRT tends to be higher in the center of the room. From the moment the window surface temperature significantly overcomes the inside face temperature of opaque surfaces, the MRT close to the window tends to be higher.

Table 4 -View Factor and Indoor Surface Temperatures: 17h

Glass	Surface	View Factor		Surface Temperature [°C]
		1.5 m from the window	center of the room	
SGU80	Window:	0.115	0.028	34.3
	Opaque surfaces:	0.878 ¹	0.976 ¹	32.4 ²
SGU30	Window:	0.115	0.028	52.4
	Opaque surfaces:	0.878 ¹	0.976 ¹	30.2 ²

Note: 1: sum of other surface view factors; and

2: average temperature of the opaque indoor surfaces.

Predicted Mean Vote (PMV) and Predicted Percentage of Dissatisfied (PPD) index

Figure 8 shows the PMV results per type of glass tested. The horizontal black line represents the acceptable thermal comfort threshold defined by the standards ASHRAE 55 (AMERICAN..., 2017), NBR 16401-2 (ABNT, 2008b), B category of ISO 7730 (INTERNATIONAL..., 2005) and II category of ISO 17772-1 (INTERNATIONAL..., 2017) and EN 16798-1 (BRITISH..., 2019).

In all scenarios, the prediction of the indoor thermal condition registered discomfort due to heat throughout the occupied period, even when in the center of the room and no adjustment was considered. The discomfort is emphasized when the solar-adjustment models are applied for a point 1.5 m from the window. Moreover, considering the occupant facing the window, the critical situation is reinforced as all models compute the subject face direction.

PMV 3.0, the Fanger model threshold, indicates a possible thermal stress condition whereby the physiological system and cognitive capacity are affected by excessive heat. In the model office SGU80, only SolarCal results did not reach this limit. By applying the CPMV and CPMV* models, PMV reaches 3.0 with most of the glazing (SGU80, IGU80, SGU50, and IGU50), at least in the solar radiation incidence peak hour. The CPMV model presented lower sensitivity to solar radiation than its correction (CPMV*) because it does not consider the diffuse portion. However, the difference between both was none or low. The maximum difference was 0.4 (SGU80 at 14h), but the divergence tends to zero, the lower the SHGC.

The dashed red lines in graphs (a) to (c) in Figure 8 show the same period whereby MRT was greater than 40 °C. Even outside the PMV-PPD applicability limit, the maximum PMV may not reach 3.0 when applying SolarCal, MSA-MRT and SA-MRT models. This happens due to the air conditioning system operating during occupancy time, which leads to low air relative humidity and airspeed fluctuation.

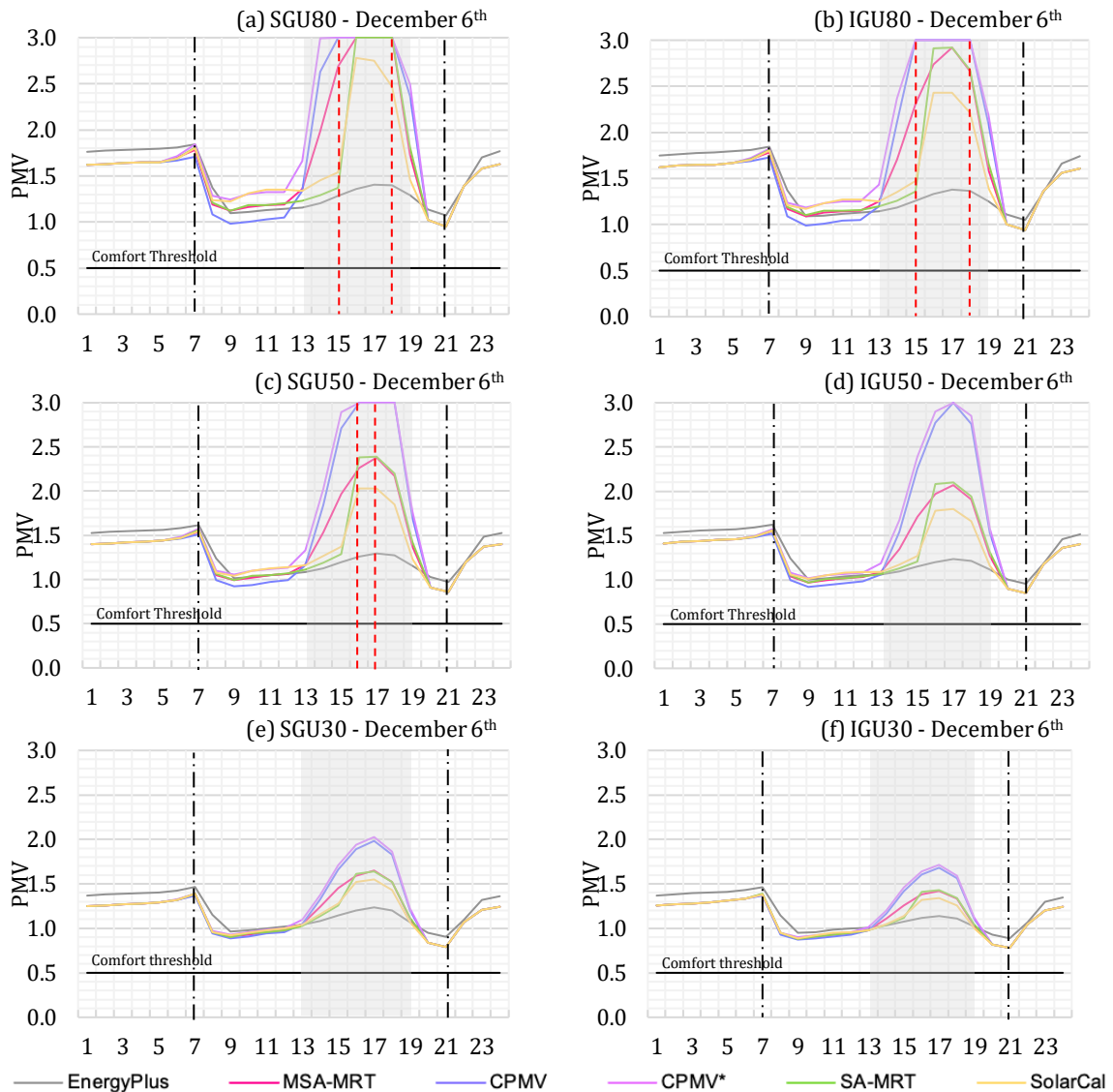
CPMV and CPMV* were more sensitive to the direct solar radiation incidence in the glazed façade, exceeding the SA-MRT up to 0.9 and the EnergyPlus up to 1.8 (IGU50 at 17h). This happens due to the adjustment that occurs by adding a new component in the heat flux calculation in PMV, and not only in the MRT. On the other hand, the PMV tends to be similar between solar-adjusted and EnergyPlus results when only diffuse solar radiation enters the room. The models' most significant difference was 0.3 between CPMV and SolarCal (SGU80 at 12h).

The SA-MRT and MSA-MRT models presented a variation of 1.6 on the PMV scale compared to EnergyPlus reports (SGU80 – 16h to 18h). By applying SolarCal, the maximum difference was 1.4. The PMV calculated with the solar-adjustment models tends to be lower than the EnergyPlus report before 8h and after 20h. This fact also is explained by the differences presented in Figure 7.

As in MRT results, the lower the glass solar transmittance, the lower the impact of the solar-adjustment model choice. The maximal hourly PMV difference among SA-MRT, MSA-MRT, and SolarCal was lower than 0.5 in 80% to 100% of the occupancy period (SGU80 and IGU80). On the other hand, if the CPMV and CPMV* results are included, the maximal hourly PMV difference among the solar-adjustment models was 1.7, which was higher than 0.5 in 40% of the occupancy period with medium SHGC (SGU50 and IGU50).

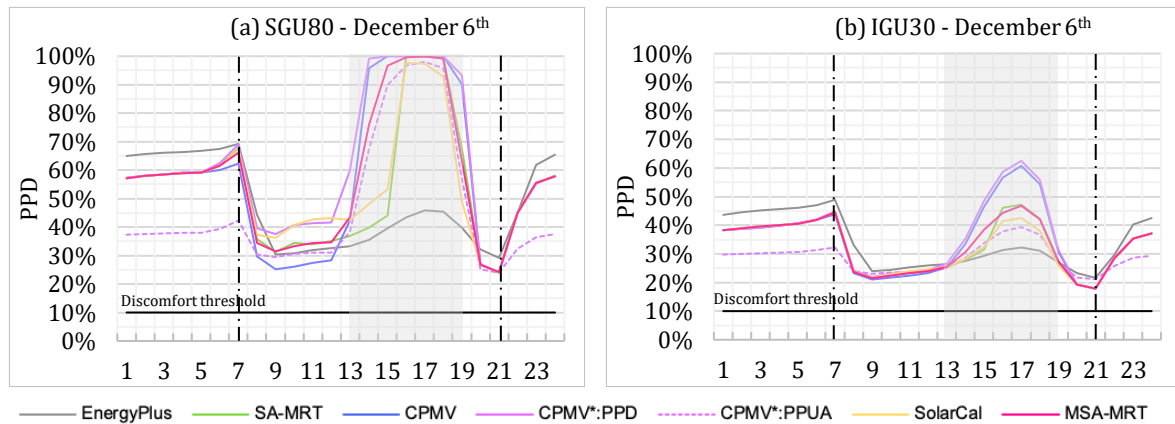
The reduction in the thermal transmittance (IGU system) also demonstrated a decrease in the solar-adjustment model choice impact. However, it was not as significant as solar transmittance impact, as the MRT analysis shows. When comparing SGU and IGU with the same base glass and solar-adjustment model, the highest divergence was 0.6 on the PMV scale (SGU80, CPMV, at 14h).

Figure 8 - PMV on December 6th in Florianópolis



PPD results followed the same pattern of PMV as the PPD is a function of PMV, except for CPMV*-PPUA. Two dissatisfied percentages were shown for the CPMV* model. CPMV*-PPD is calculated by replacing the PMV for CPMV* in the original PPD equation. CPMV*-PPUA is the unacceptable percentage, defined through a correlation based on the results of surveys and measurements obtained in the experiment carried out by Zhang *et al.*(2020). Although CPMV* showed the highest PMV indices, the dissatisfied percentage is drastically reduced using the PPAU index. At 14h, the difference among CPMV*-PPD and CPMV*-PPUA reached 36 percentage points with SGU80 at 19h and 23 p.p. with IGU30 at 17h (Figure 9).

Zhang *et al.*(2020) substantiated that the results of the in loco experiment indicated wide variability in the solar radiation acceptance and people tend to tolerate better the solar radiation presence than the high air temperature. However, the PPAU was developed using thermal votes obtained in only one city in China, namely Tianjin. It is understood that cultural factors and adaptation to this specific climate are decisive for these results. Developing the index for other climates to be reasonable using PPAU in thermal comfort prediction would be necessary.

Figure 9 - PPD on December 6th in Florianópolis

Radiant temperature asymmetry

Complementary to the thermal comfort conditions analysis, it is also essential to observe the possibility of local discomfort due to the radiant temperature asymmetry when the window effects are assessed. Among the solar adjustment models tested, only CPMV and CPMV* do not suggest any correction regarding the contribution of short-wave radiation in the plane radiant temperature. Figure 10 presents the radiant asymmetry results per glass type, and Figure 11 presents the percentage of local discomfort (PD) by radiant temperature asymmetry due to hot walls. Horizontal black lines indicate asymmetry in the radiant temperature threshold established by standards (ABNT, 2008b; AMERICAN..., 2017; BRITISH..., 2019; INTERNATIONAL..., 2005, 2017). In both figures, the asymmetry results without any solar adjustment can be observed in position 1.5 m distant from the window (continuous gray line) and in the center of the room (dashed gray line).

In contrast to the solar-corrected PMV, PPD, and MRT results, the MSA-MRT model shows higher sensitivity to solar radiation exposition and the glass type in the radiant temperature asymmetry. The SolarCal presented the second largest sensitivity. However, the radiant asymmetry calculated by applying the MSA-MRT model was up to 19 °C higher than with SolarCal (SGU80, at 15h), and the maximum PD difference was 11 p.p. (SGU80, at 17h).

At first, it is odd that an environment, despite being conditioned, that remains completely outside the thermal comfort zone during the occupied period does not present discomfort due to radiant temperature asymmetry with most solar adjustment models. Additionally, there are moments when the sun is positioned in front of the occupant in the late afternoon.

Nonetheless, the temperature of opaque indoor surfaces remained constantly above 25.5 °C all day long (Figure 6), which may be related to the adiabatic set of the internal walls, ceiling, and floor. These values indicate that the surfaces did not go into thermal balance with the indoor air temperature (24 °C) at any moment while the room was occupied. Therefore, the delta radiant temperature between the planes is reduced.

When no solar adjustment is considered, the asymmetry radiant results for a person 1.5 m distant from the window indicated coherence with the glass indoor surface temperature (Figure 6), higher in the office with a selective glazing system. However, when the solar-adjustment models are applied, the asymmetry tends to increase as solar radiation incidence increases. In the latter case, the radiant asymmetry was significantly higher in the SGU80, and IGU80 offices, presenting the highest solar transmittance and admitting more direct solar radiation. In this scenario, the glass solar transmittance tends to have a higher impact on the prediction of radiant temperature asymmetry than the solar absorptance and the temperature of the surrounding surfaces. This situation occurs due to the importance given to the diffuse and beam solar radiation ratios in the radiant temperature asymmetry weighting in the solar-adjustment models.

Figure 10 - Radiant temperature asymmetry on December 6th in Florianópolis

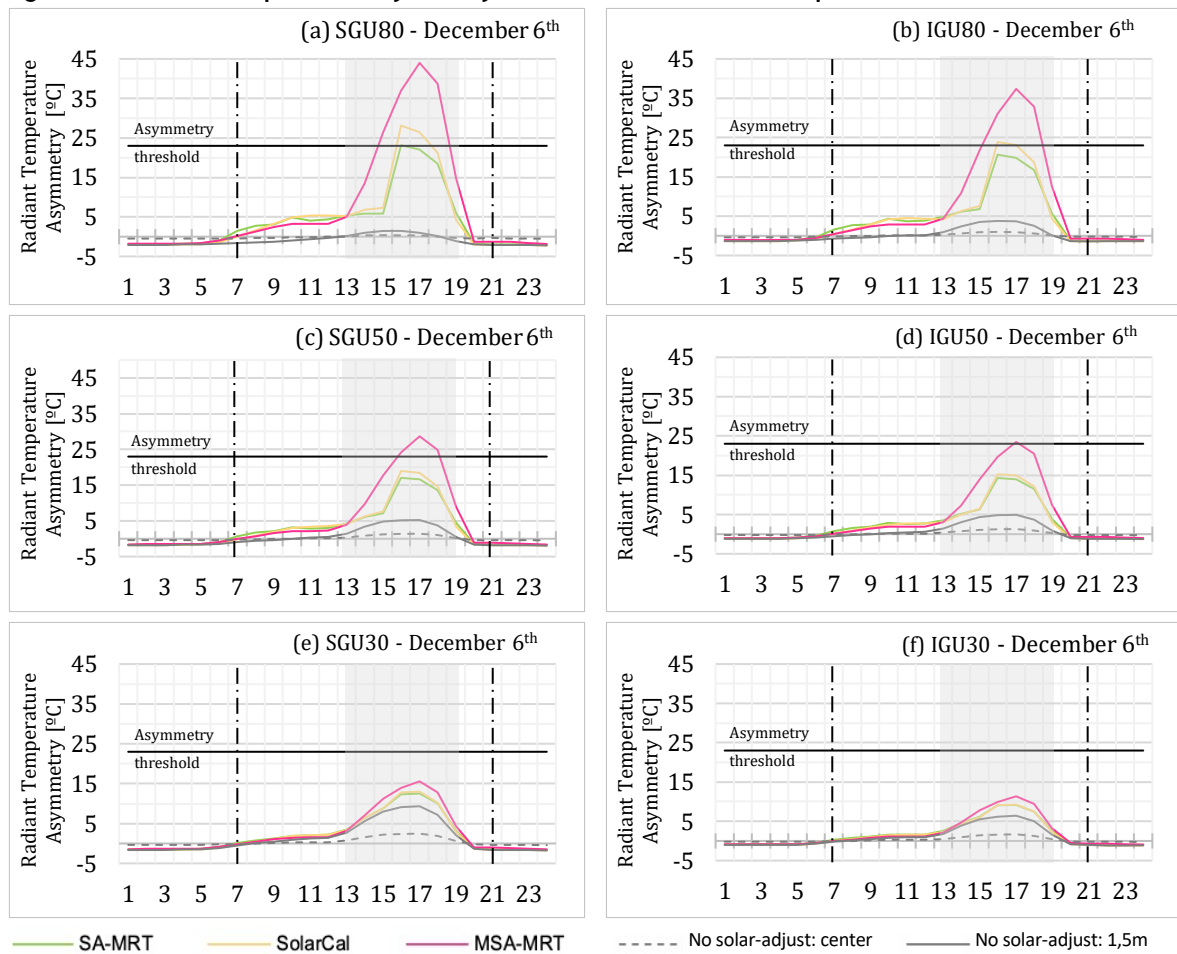
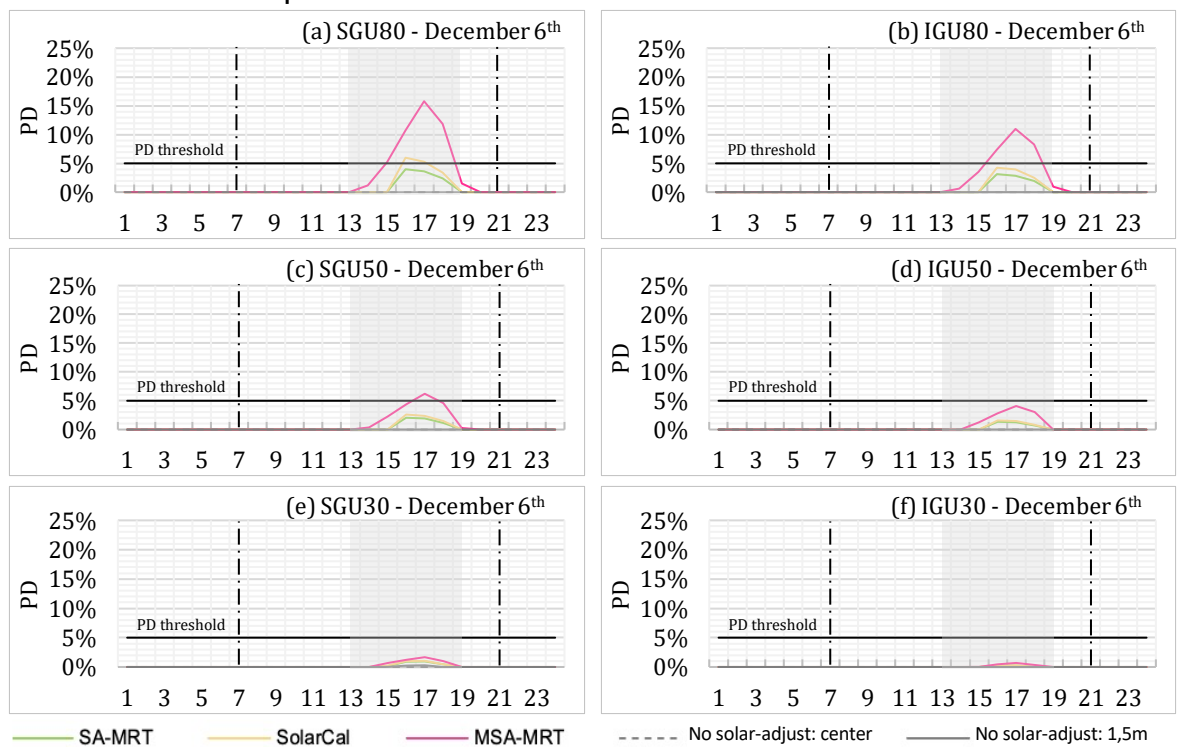


Figure 11 - Percentage of local discomfort for asymmetry in radiant temperature due to hot walls on December 6th in Florianópolis



Summer day with low solar radiation incidence and winter day with high solar radiation incidence

Two more days, with different interrelations between the outdoor temperature and solar radiation incidence were analyzed. January 15th presents a similar temperature throughout the day compared to December 6th, but a lower incidence of solar radiation in the West façade (up to 460 W/m² hourly). In turn, on June 26th lower temperatures were maintained than on December 6th, but a high solar radiation incidence for the winter season.

On January 15th, the diffuse solar radiation represented the most significant fraction of the solar radiation in the West façade. The results for this day reinforce the sensitivity of the SolarCal model to the diffuse solar radiation and its low impact in the MSA-MRT model, as exemplified in Figure 12. However, in this context, the SA-MRT model showed higher sensitivity to the diffuse radiation than observed on December 6th. These correlations are evident when comparing these MRT results with the shape of incident sky diffuse solar radiation in Figure 2b.

Due to the high external temperatures, the environment starts the workday in a condition of heat discomfort, regardless of the type of glass (PMV between 2.0 and 2.6), as exemplified in Figure 13 for the SGU80 and IGU80 models. This discomfort remained throughout the whole occupied period. However, as there is less beam solar radiation incidence, the peak of discomfort with most solar-adjustment models (SA-MRT, MSA-MRT, and SolarCal) is up to 0.4 (or 31 p.p. in PPD) higher than the EnergyPlus results (SGU80, 16h, Figure 13). It is four times less than on December 6th. Likewise, on December 6th, the CPMV and CPMV* models presented higher PMV and PPD results, up to 0.7 (or 36 p.p.) and 1.2 (or 51 p.p.) over EnergyPlus, respectively. Nevertheless, CPMV and CPMV* presented a significant difference on January 15th, conversely to December 6th. During the peak time, by applying the CPMV*, the PMV was 0.5 higher than by CPMV. The difference in PPD was 15 p.p. The low incidence of solar radiation on the West façade on this day and the prevalence of diffuse radiation explain both findings.

While the outdoor temperature during the occupied period on December 6th remained between 23°C and 30 °C on the winter day (June 26th), it was between 12 °C and 18°C (Figure 2c). Despite the 12 °C peak temperature divergence, the MRT peak calculated by EnergyPlus was up to 3 °C lower on the winter day. By applying the solar-adjustment models, the maximum difference occurred in the office with SGU80 (10°C, MSA-MRT –Figure 14a) and the minimum happened with IGU30 (2.5 °C, SolarCal–Figure 14b). Besides the lower temperatures, the MRT reached up to 44.5 °C (SGU80, SA-MRT, 16h) due to the high incidence of solar radiation on the windows.

Although the outdoor temperature was always under the heating setpoint, the room presented a condition of discomfort for heat during the whole occupied period regardless of the glass thermal properties, as exemplified in Figure 15. The PPD due to heat was up 100% by applying CPMV and CPMV*, which means almost 75 p.p. more than the PPD calculated by EnergyPlus (SGU80, 16h). SolarCal presented the lowest difference with EnergyPlus results; however, it was still about 45 p.p. higher.

The results of radiant temperature asymmetry on January 15th and June 26th did not present a significant difference in the patterns found on December 6th or described above.

Figure 12 - Mean Radiant Temperature on February 15th in Florianópolis

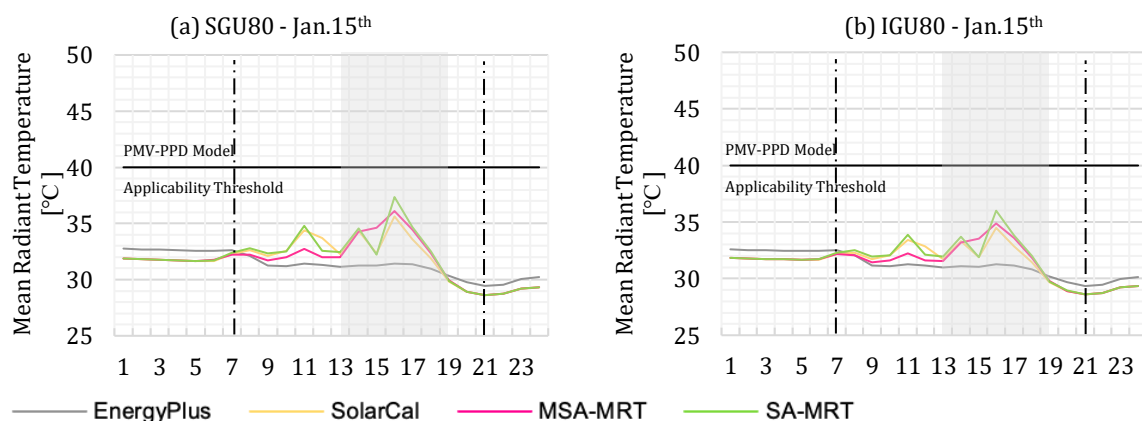


Figure 13 - (a) PMV and (b) PPD on February 15th in Florianópolis

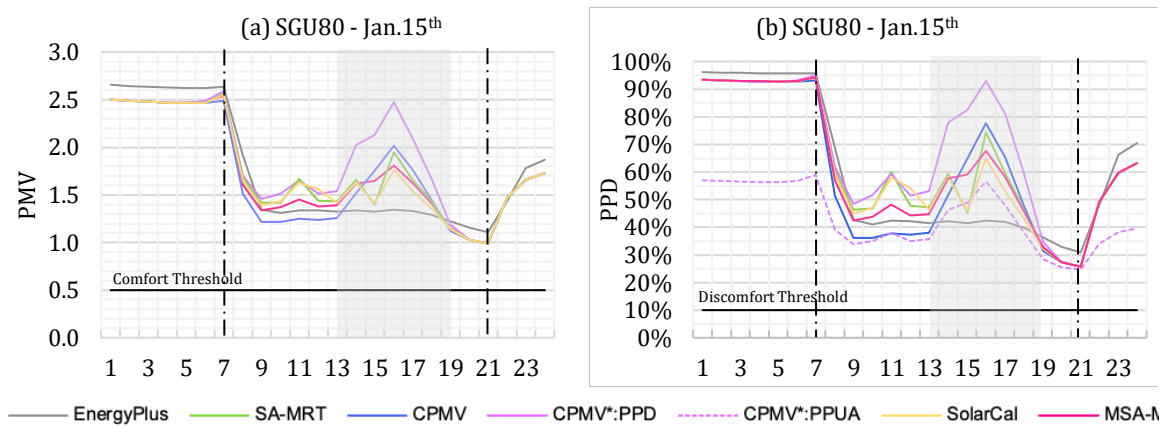


Figure 14 - Mean Radiant Temperature on June 26th in Florianópolis

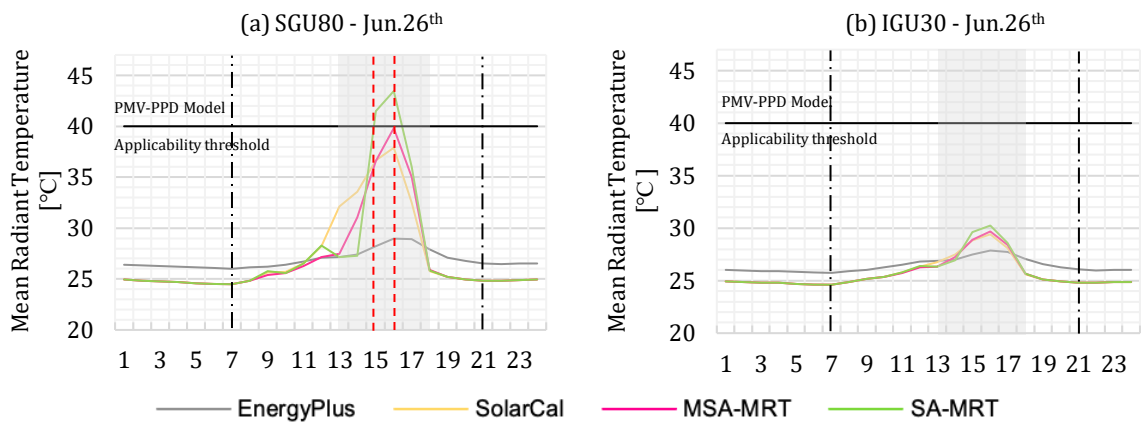
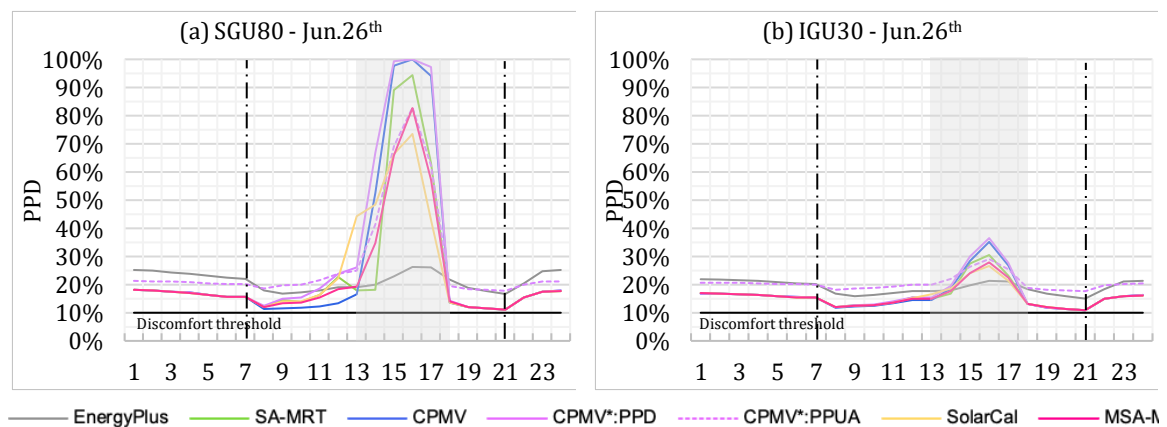


Figure 15 - PPD on June 26th in Florianópolis



Discussion

In the period with beam solar radiation incidence in the West façade (from 13h to 19h), a steep rise in MRT was noticed in the three models. However, this curve started to escalate at 14h with the MSA-MRT model, while it started at 16h in SA-MRT and SolarCal models. The same occurred in PMV, in which CPMV and CPMV* results started to rise at 13h and 14h, respectively. This lag derives from the coefficients applied to SA-MRT and SolarCal, which indicate if the person (or point in the room) is being reached by the solar beam radiation entering the window.

The calculation procedure of SA-MRT defines if the subject is in the direct solar radiation incidence area (sunspot) in the indoor space through trigonometry considering the solar angles. This procedure defines C_S^{in} , the inner building shading coefficient, which counts as 1 when the beam solar radiation reaches the subject and 0 otherwise. Then, the coefficient is included in the component of MRT. This brings a significant advantage compared with the other models as it enables one to accurately define if the solar radiation reaches the occupant of a specific place in the indoor space in a given time. It also eases the hourly calculation for extended periods (e.g., monthly, seasonally, annually).

SolarCal model also applies a coefficient to define if the beam solar radiation reaches the occupant: the fraction of body exposed to sunlight (f_{bes}). This coefficient is defined as the fraction of the body projected area factor (f_p) not shaded by any indoor surroundings. f_{bes} is 1 when the subject is completely exposed and 0 when shaded. However, this value can be estimated in a simplified way, and there is no calculation procedure for this. Unlike C_S^{in} , f_{bes} is not a binary factor, which may be advantageous as it admits that the beam solar radiation reaches only a fraction of the body area facing the window direction.

Due to the MSA-MRT model including the solar radiation flux from the reflection of short-wave radiation on the floor and the opaque indoor surfaces, we expected that this model would present higher MRT values than the SA-MRT model. However, the MRT values with MSA-MRT tend to be similar to SA-MRT except for the period between 14h and 16h, when MSA-MRT was 12 °C higher than SA-MRT due to MSA-MRT not including a body shading/exposure coefficient.

The low weight of the reflections from the floor could be associated with solar altitude. According to Lambert's Cosine Law, the fraction of normal beam radiant energy received on a horizontal surface reduces as long as the solar altitude decreases. The highest beam solar irradiance occurred at 17h on the West façade, when the solar altitude is 28.2°. Consequently, the fraction of this radiation received on the floor is approximately 50%. Therefore, the increase due to the component of solar radiation flux from the reflection of short-wave radiation in the MSA-MRT model is less significant in analysing a West glazed façade. However, the MRT should still result in higher values with the MSA-MRT model than the SA-MRT.

It is suggested that this occurrence may arise from the calculation method in SA-MRT. In these models, the fraction of diffuse and direct solar radiation that enters through the window is estimated based on the horizontal global radiation, climate data, and solar geometry, which result in significant uncertainties, mainly about the coefficients needed.

In contrast, MSA-MRT does not present a calculation procedure for the radiation intensity calculation, which places the use of EnergyPlus output data of solar radiation transmitted through the window in the present study. As a result, the beam solar radiation crossing the glazed surface results in higher values through SA-MRT calculation.

Various authors (DERVISHI; MAHDAVI, 2012; HUANG; ZHAI, 2020; JACOVIDES *et al.*, 2006) indicated that calculation models of solar irradiation diffuse fraction, mainly derived from the horizontal global irradiation, tend to present higher error levels in low solar altitude conditions. Consequently, the results obtained by solar-adjustment models also carry these errors. Although the radiation incidence peak occurred when the solar altitude was 28.2° in the present study, it is understood that the results are still significant since previous studies suggested that these models lead to a more significant error percentage when the solar altitude is lower than 20° (DERVISHI; MAHDAVI, 2012; HUANG; ZHAI, 2020).

The elevated MRT values estimated by applying SA-MRT contradict the results found by Huang and Zhai (2020), which compared results obtained with nine solar-adjust models for an office room in Lhasa, Tibet. Among the MRT correction models, the SA-MRT model presented the smallest convergence with loco measurements and tended to underestimate the MRT. This divergence is presumably related to the local climate – Köppen-Geiger Dwc, snowy weather with a dry winter and cold summer. It may also be a result of the limitations of this study previously described.

Likewise, the findings of Huang and Zhai (2020) indicated that the PMV results by applying the CPMV model differ significantly from measurements and underestimate the solar radiation impact. The present study indicates the opposite. Even though the CPMV model does not consider the diffuse radiation effects, PMV and PPD adjusted with this model were significantly higher than in other models. The results indicated that the model developed by Zhang *et al.* (2018, 2020) might overestimate the solar radiation effect on occupants' thermal perception and comfort in temperate climates, as in Florianópolis. The models were tested only in the climate context of Tianjin, China, which is characterized by hot and humid summers and cold and dry winters (Dwa in Köppen-Geiger Scale). This fact may impact the model validation.

Besides the climate type, another possible reason for the significantly higher PMV results by applying CPMV and CPMV* may be related to the weight of the beam and diffuse solar radiation components in the CPMV* calculation method. Instead of modifying the radiation heat exchange parcel in the PMV equation, the author added two components aside from the six environmental and personal parameters. In the PMV equation, the radiation sensitive heat loss component is expressed in terms of the radiation heat transfer coefficient and the difference between the mean temperature of the outer surface of the clothed body and the mean radiant temperature by long waves. The beam and diffuse components of the solar radiation heat gain proposed by Zhang *et al.* (2018, 2020), in turn, did not undergo any balance. Consequently, the influence of radiant heat transfer on the body heat balance is significantly increased.

The relation between MRT results, window surface temperature, and transmission properties of the glass indicated a significant impact of the solar radiation admission control on the predicted occupants' thermal comfort in workstations located close to windows, more importantly in conditions of outside air temperature between 20 °C and 30 °C and high solar radiation incidence. This pattern is maximized when a solar adjustment model is applied for comfort calculation. However, it also occurs in comfort prediction calculated by EnergyPlus, but more subtly. The radiant temperature asymmetry results also indicated that when a solar adjustment model is applied, the SHGC tends to have a more significant impact on the prediction of occupant thermal discomfort.

In all scenarios analyzed, the solar-adjustment models tend to present similar results to EnergyPlus when using lower SHGC glass, i.e., with less solar radiation gain. Consequently, the results of the solar adjustment models tend to approach the results calculated by EnergyPlus, which considers only the longwave radiation.

In general, the three days presented similar patterns and supported the analysis for the summer day with the highest solar radiation incidence. When comparing the results for these three days, the significant impact on the occupant thermal comfort indices is highlighted when correcting the effect of the solar radiation. A room tends to present an increase in the conditions of discomfort due to heat when there is high solar radiation incidence, even on winter days.

Conclusions

The present study compared the results of thermal comfort indices corrected by four adjustment models of the solar radiation effect on people's thermal comfort. It focused on occupants located in workstations nearby the windows in office buildings with a highly glazed façade.

The PMV results obtained with CMPV/CPMV* models were drastically higher than other models, and controversy indicated lower thermal discomfort indices. The MSA-MRT model presented PMV and MRT similar to the SA-MRT, although it considers the reflections of shortwave radiation on internal opaque surfaces. In contrast, MSA-MRT reported the most significant asymmetry in radiant temperature, differing significantly from the other models. These facts indicate relevant inconsistencies in both models.

The SA-MRT and SolarCal models showed seemingly more coherent results, with the values adjusted by SolarCal lower. SA-MRT models are more detailed about solar and space geometry, but the procedure for calculating the solar radiation entering through the window may comprehend inaccuracies. On the other hand, the SolarCal model is simpler to implement, whereas both presented similar results.

The current study does not relate the adjusted thermal comfort indices with measurement data or people's thermal perception in a realistic environment. Consequently, it cannot be concluded which model is higher correlated with reality. Moreover, there is still no benchmark for the comparison between the results of each model. However, there is still a lack of discussions about applying the various solar adjustment models and the consequences of choosing between them. Therefore, the present study enlarges this discussion and numerically indicates the limitations and advantages of each solar-adjust model in the context of a temperate climate in South America.

References

- AMERICAN SOCIETY OF HEATING, REFRIGERATING AND AIR-CONDITIONING ENGINEERS. **Standard 55**: thermal environmental conditions for human occupancy. Atlanta, 2017.
- ARENS, E. *et al.* Modeling the comfort effects of short-wave solar radiation indoors. **Building and Environment**, v. 88, p. 3–9, 2015.
- ASSOCIAÇÃO BRASILEIRA DE NORMAS TÉCNICAS. **NBR 16401-1**: instalações de ar-condicionado: sistemas centrais e unitários: parte 1: projetos das instalações. Brasília, 2008a.

ASSOCIAÇÃO BRASILEIRA DE NORMAS TÉCNICAS. **NBR 16401-2**: instalações de ar-condicionado: sistemas centrais e unitários: parte 2: parâmetros de conforto térmico. Brasília, 2008b.

BAVARESCO, M. V.; GHISI, E. Influência da interação dos usuários com elementos internos de sombreamento no consumo energético de edificações comerciais. In: ENCONTRO NACIONAL DE CONFORTO NO AMBIENTE CONSTRUÍDO, 14.; ENCONTRO LATINO AMERICANO DE CONFORTO NO AMBIENTE CONSTRUÍDO, 10., Camboriú: Marketing Aumentado, 2017. **Anais [...]** Camboriú, 2017.

BESSOUDO, M. *et al.* Indoor thermal environmental conditions near glazed facades with shading devices: part I: Experiments and building thermal model. **Building and Environment**, v. 45, n. 11, p. 2506–2516, 2010.

BRITISH STANDARD. **EN 16798-1**: energy performance of buildings: part 1: indoor environmental input parameters for design and assessment of energy performance of buildings addressing indoor air quality, thermal environment, lighting and acoustics: module M1-6. Bussels, 2019.

CAPPELLETTI, F. *et al.* Passive performance of glazed components in heating and cooling of an open-space office under controlled indoor thermal comfort. **Building and Environment**, v. 72, p. 131–144, 2014.

DERVISHI, S.; MAHDAVI, A. Computing diffuse fraction of global horizontal solar radiation: a model comparison. **Solar Energy**, v. 86, n. 6, 2012.

GASPARELLA, A. *et al.* Analysis and modelling of window and glazing systems energy performance for a well insulated residential building. **Energy and Buildings**, v. 43, n. 4, p. 1030–1037, 2011.

HAWILA, A. A.-W. W. *et al.* An analysis of the impact of PMV-based thermal comfort control during heating period: A case study of highly glazed room. **Journal of Building Engineering**, v. 20, p. 353–366, 2018.

HUANG, L.; ZHAI, Z. Critical review and quantitative evaluation of indoor thermal comfort indices and models incorporating solar radiation effects. **Energy and Buildings**, v. 224, p. 110204, 2020.

HUANG, Y.; NIU, J. L.; CHUNG, T. M. Comprehensive analysis on thermal and daylighting performance of glazing and shading designs on office building envelope in cooling-dominant climates. **Applied Energy**, v. 134, p. 215–228, 2014.

INTERNATIONAL ORGANIZATION FOR STANDARTIZATION. **ISO 17772-1**: energy performance of buildings: indoor environmental quality: part 1: indoor environmental input parameters for the design and assessment of energy performance of buildings. Geneve, 2017.

INTERNATIONAL ORGANIZATION FOR STANDARTIZATION. **ISO 7726**: ergonomics of the thermal environment: instruments for measuring physical quantities. Geneve, 1998.

INTERNATIONAL ORGANIZATION FOR STANDARTIZATION. **ISO 7730**: ergonomics of the thermal environment: analytical determination and interpretation of thermal comfort using calculation of the PMV and PPD indices and local thermal comfort criteria. Geneve, 2005.

INTERNATIONAL ORGANIZATION FOR STANDARTIZATION. **ISO/TR 17772-2**: energy performance of buildings: overall energy performance assessment procedures: part 2: guideline for using indoor environmental input parameters for the design and assessment of energy performance of buildings. Geneve, 2018.

JACOVIDES, C. P. *et al.* Comparative study of various correlations in estimating hourly diffuse fraction of global solar radiation. **Renewable Energy**, v. 31, n. 15, 2006.

KOTTEK, M. *et al.* World Map of the Köppen-Geiger climate classification updated. **Meteorologische Zeitschrift**, v. 15, n. 3, p. 259–263, 10 jul. 2006.

LA GENNUSA, M. *et al.* A model for managing and evaluating solar radiation for indoor thermal comfort. **Solar Energy**, v. 81, n. 5, p. 594–606, 2007.

LA GENNUSA, M. *et al.* The calculation of the mean radiant temperature of a subject exposed to the solar radiation - A generalised algorithm. **Building and Environment**, v. 40, n. 3, p. 367–375, 2005.

LAWRENCE BERKELEY NATIONAL LABORATORY. **Window**. Versão 7.7.10. Berkeley, 2020.

MARINO, C. *et al.* A generalized model of human body radiative heat exchanges for optimal design of indoor thermal comfort conditions. **Solar Energy**, v. 176, p. 556–571, oct. 2018a.

- MARINO, C. *et al.* A generalized model of human body radiative heat exchanges for optimal design of indoor thermal comfort conditions. **Solar Energy**, v. 176, p. 556–571, oct. 2018b.
- MARINO, C. *et al.* The effect of the short wave radiation and its reflected components on the mean radiant temperature: modelling and preliminary experimental results. **Journal of Building Engineering**, v. 9, p. 42–51, 2017a.
- MARINO, C. *et al.* The effect of the short wave radiation and its reflected components on the mean radiant temperature: modelling and preliminary experimental results. **Journal of Building Engineering**, v. 9, p. 42–51, 2017b.
- MARINO, C. *et al.* The spatial evaluation of the radiative human body heat exchanges: an effective contribution for limiting energy consumption and achieving better indoor conditions in buildings. **Journal of Building Engineering**, v. 16, p. 118–128, 2018c.
- MARINO, C.; NUCARA, A.; PIETRAFESA, M. Thermal comfort in indoor environment: effect of the solar radiation on the radiant temperature asymmetry. **Solar Energy**, v. 144, p. 295–309, 2017.
- PINTO, M. M.; WESTPHAL, F. S. Vidro insulado em escritórios com fachada envidraçada em Florianópolis (SC). In: ENCONTRO NACIONAL DE CONFORTO NO AMBIENTE CONSTRUÍDO, 15.; ENCONTRO LATINO-AMERICANO DE CONFORTO NO AMBIENTE CONSTRUÍDO, 11., João Pessoa, 2019. **Anais [...]** João Pessoa, 2019.
- TARTARINI, F. *et al.* CBE thermal comfort tool: online tool for thermal comfort calculations and visualizations. **SoftwareX**, v. 12, p. 100563, 2020.
- THORSSON, S. *et al.* Different methods for estimating the mean radiant temperature in an outdoor urban setting. **International Journal of Climatology**, v. 27, p. 1983–1993, 2007.
- TZEMPELIKOS, A. *et al.* Indoor thermal environmental conditions near glazed facades with shading devices: part II: thermal comfort simulation and impact of glazing and shading properties. **Building and Environment**, v. 45, n. 11, p. 2517–2525, 2010.
- U.S. DEPARTMENT OF ENERGY. **EnergyPlus**. Version 8.9.0. USA, 2020.
- U.S. DEPARTMENT OF ENERGY. **Weather data**.USA, 2019. Available: <https://energyplus.net/weather>. Access: 18 mar. 2019.
- ZHANG, H. *et al.* The CPMV index for evaluating indoor thermal comfort in buildings with solar radiation. **Building and Environment**, v. 134, p. 1–9, 2018.
- ZHANG, H. *et al.* The CPMV* for assessing indoor thermal comfort and thermal acceptability under global solar radiation in transparent envelope buildings. **Energy and Buildings**, v. 225, p. 110306, 2020.
- ZOMORODIAN, Z. S.; TAHSILDOOST, M. Assessment of window performance in classrooms by long term spatial comfort metrics. **Energy and Buildings**, v. 134, p. 80–93, 2017.
- ZYGMUNT, M.; GAWIN, D. Analysis of energy efficiency and thermal comfort for an office building complex located in Poland: a case study. **IOP Conference Series: Materials Science and Engineering**, v. 415, p. 12023, 2018.

Mônica Martins Pinto

Laboratório de Conforto Térmico, Departamento de Arquitetura e Urbanismo | Universidade Federal de Santa Catarina | Campus UFSC, Trindade, PósARQ/CTC | Caixa Postal 478 | CEP 88040-900 | Florianópolis - SC - Brasil | Tel.: (48) 3721-4974 | E-mail: monicamartinspinto@outlook.com

Fernando Simon Westphal

Laboratório de Conforto Térmico, Departamento de Arquitetura e Urbanismo | Universidade Federal de Santa Catarina | E-mail: fernando.sw@ufsc.br

Ambiente Construído

Revista da Associação Nacional de Tecnologia do Ambiente Construído

Av. Osvaldo Aranha, 99 - 3º andar, Centro

Porto Alegre - RS - Brasil

CEP 90035-190

Telefone: +55 (51) 3308-4084

www.seer.ufrgs.br/ambienteconstruido

www.scielo.br/ac

E-mail: ambienteconstruido@ufrgs.br



This is an open-access article distributed under the terms of the Creative Commons Attribution License.